Progress In Electromagnetics Research, Vol. 109, 301–324, 2010

FAST ANALYSIS OF MICROSTRIP ANTENNAS OVER A FREQUENCY BAND USING AN ACCURATE MOM MATRIX INTERPOLATION TECHNIQUE

Y. Chen, S. Yang, S. He, and Z. Nie

Department of Microwave Engineering
School of Electronic Engineering
University of Electronic Science and Technology of China (UESTC)
Chengdu 611731, China

Abstract—A novel method based on the hybrid volume-surface integral equation (VSIE) and the impedance matrix interpolation technique is presented for the fast analysis of microstrip antennas in frequency sweeps. A novel impedance matrix interpolation scheme is extended to the impedance matrix associated with VSIE, thus providing high accuracy, high efficiency, and large interpolation bandwidth for metal-dielectric composite problems. To demonstrate the effectiveness and accuracy of the proposed technique, numerical results for typical rectangular patch antennas and a broadband U-slot rectangular patch antenna are presented. Good agreement among the interpolation results, the exact method of moments (MoM) solutions, the finite element method (FEM) solutions, and measured data is observed over the bandwidth. The interpolation bandwidth is further investigated through a scattering problem. Numerical results show that high accuracy is obtainable within 10 : 1 bandwidth.

1. INTRODUCTION

The frequency domain integral equation approach is one of the most popular methods for the analysis of microstrip antennas, due to the fact that it usually achieves more accurate results than differential equation solvers such as the finite-difference time-domain (FDTD) method [1–9]. Among various integral equation approaches, the surface integral equation (SIE) approach is often used for the analysis of

Received 11 August 2010, Accepted 28 September 2010, Scheduled 25 October 2010
Corresponding author: Y. Chen (yikaichen@uestc.edu.cn).

microstrip antennas, where the multilayer medium Green's function is employed to take into account the effect of the dielectric substrate and ground plane [10–14]. The major advantage of the SIE approach is its lower memory requirement, since basis functions are only assigned on conducting patches. However, the ground and substrate are considered to be infinite in transverse directions. It is generally understood that when the substrate edge is close to the radiating patch, the calculated input impedance and radiation patterns will be inaccurate. Moreover, the trend toward miniaturization of electronic devices requires the dimensions of antennas to be as small as possible. Therefore, the assumption of infinite ground plane and substrate is no longer appropriate. As another type of surface integral equation method, the PMCHWT (Poggio, Miller, Chang, Harrington, Wu, and Tsai) method can be used to analyze problems with finite size substrates [15–19]. However, some limitations are inherent in the PMCHWT method, which will prevent its wide use in microstrip antenna analysis. Firstly, since appropriate Green's functions are required to represent the homogeneous material domains, the PMCHWT method can only handle problems with piecewise homogeneous materials [20]. Secondly, if the dielectric substrate is overlapped or touched with perfect electric conducting (PEC) surface, an appropriate junction resolution process is required to meet the special boundary condition at the interface, which will increase the difficulty of practical application [21–25]. Finally, the PMCHWT method always suffers from poor convergence problem, especially when high contrast materials are involved [26].

In this paper, the hybrid volume-surface integral equation (VSIE) approach [6] is employed to analyze microstrip antennas on finite size dielectric substrate and ground plane. In this method, the entire structure comprising the patch, ground plane, feed structure, and dielectric substrate are assigned with basis functions. The surface currents on the PEC surface and the volume currents in the dielectric substrate are obtained by solving the VSIE via the method of moments (MoM). Other parameters of interests in radiation problems such as the input impedance, directivity, and radiation patterns can be readily obtained from the solved currents. As compared with the PMCHWT method, the VSIE method generally requires larger number of unknowns for problems with single substrate material. However, it is not a serious problem in this paper, since the number of unknowns involved in microstrip antenna analysis is very small. Moreover, in the PMCHWT method, each interface must be meshed in a stratified medium situation, leading to a significant increase in the number of unknowns. Furthermore, the VSIE method has the flexibility and capability of handling inhomogeneous and anisotropic

material [26]. Finally, since the free-space Green's function is used in the VSIE method, it is much easier to be integrated with various fast algorithms, such as the multilevel fast multipole algorithm [20]. On the other hand, we have also realized that once dielectric substrate with high permittivity is involved, the convergence rate in VSIE will be much slower than the PMCHWT method. However, the basic antenna design principle tells us that high permittivity dielectric is rarely employed in wideband antenna designs, since high permittivity dielectric material will increase the antenna Q-value greatly, and eventually limited the operating bandwidth. Considering the advantages and limitations of the two methods, we will not use the PMCHWT method for wideband microstrip antenna analysis, since wideband stacked microstrip antennas and microstrip antennas fabricated on inhomogeneous and anisotropic material are widely used in modern communication systems.

Independent of the type of integral equation we used, the major limitation of MoM is always being the long CPU time required for the impedance matrix computation, since it will consume a considerable portion of the total solution time [12]. This limitation becomes more serious in the volume-surface integral equation approach, due to the fact that the volume occupied by the dielectric material is also meshed, and the number of unknowns is increased significantly. Therefore, if the frequency response of any parameter over a wide frequency band is required, one has to repeat the impedance matrix filling at each frequency sample point, and the MoM would be rather time consuming.

One promising approach to speed up the impedance matrix filling is the impedance matrix interpolation technique [12, 27–33]. Various interpolation techniques such as the quadratic polynomial interpolation [12, 27–29], Hermite interpolation [30], Lagrange interpolation [31], and their improved versions are introduced briefly and commented reasonably in [32]. In this paper, the accurate and efficient interpolation technique in [32] is extended to the VSIE formulations for the fast analysis of microstrip antennas.

The rest of this paper proceeds as follows. Formulations of the interpolation scheme in VSIE are presented in Section 2, where the modified matrix elements and their first derivative will be derived. To keep the integrity of the paper, the cubic polynomial interpolation technique with first order derivative coefficient is also presented. In Section 3, numerical results for probe fed rectangular patch antennas and a broadband U-slot patch antenna are compared with those of the exact MoM solutions. Measured data and FEM solutions obtained from the commercial software Ansoft HFSS are also provided for comparison. Finally, the interpolation bandwidth is illustrated

by considering the scattering from a coated PEC sphere in a wide frequency band. Conclusions are given in Section 4.

2. FORMULATIONS

2.1. Formulations for the Volume-Surface Integral Equation

The general configuration of a microstrip antenna is shown in Fig. 1. It consists of a radiating patch fed with a coaxial probe, a finite dielectric substrate, and a finite ground plane. For simplicity, it is assumed that the dielectric material for the substrate has piece-wise continuous relative permittivity ε_r and permeability $\mu = \mu_0$, although this assumption is not necessary for the VSIE method. The metal-dielectric composite object shown in Fig. 1 contains the dielectric volume V and perfect conducting surface $S = S_{patch} + S_{ground} + S_{probe}$, where S_{patch}, S_{ground}, and S_{probe} are the surfaces of the patch, ground plane, and probe, respectively. By the equivalence principle, the total electric field in dielectric volume V consists of the incident field $\vec{E}^{\,i}(\vec{r})$ and scattering field produced by the equivalent surface current $\vec{J}_S$ and equivalent volume current $\vec{J}_V$. Thus, the electric field volume integral equation can be written as

$$\vec{E}^{\,i}(\vec{r}) = \vec{E}(\vec{r}) - \vec{E}^{\,sca}\left(\vec{r}; \vec{J}_S\right) - \vec{E}^{\,sca}\left(\vec{r}; \vec{J}_V\right) \quad \vec{r} \in V \qquad (1)$$

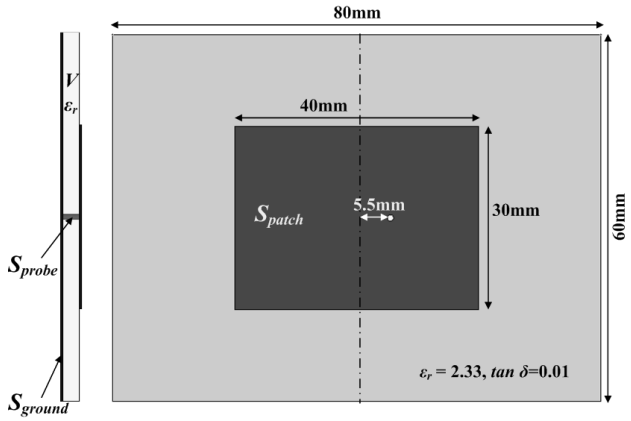

Figure 1. Configuration of a rectangular patch antenna (Antenna #1).

where $\vec{E}(\vec{r})$ is the total field in the dielectric volume, $\vec{E}^{sca}(\vec{r};\vec{J}_\alpha)$ is the scattered field in the dielectric volume due to the sources $\vec{J}_\alpha$, $\alpha = S, V$.

The boundary condition on the PEC surface S requires that the tangential component of the total electric field vanishes on the surface. Thus, the following surface integral equation can be obtained

$$\vec{E}^{i}_{\tan}(\vec{r}) = -\left[\vec{E}^{sca}\left(\vec{r};\vec{J}_S\right) + \vec{E}^{sca}\left(\vec{r};\vec{J}_V\right)\right]_{\tan} \quad \vec{r} \in S \tag{2}$$

where the subscript 'tan' represents the tangential component of the vector.

The total electric field $\vec{E}(\vec{r})$ in the dielectric volume is related to the induced volume current by

$$\vec{J}_V(\vec{r}) = i\omega\varepsilon_0\left(1-\varepsilon_r\right)\vec{E}(\vec{r}) = i\omega\chi(\vec{r})\vec{D}(\vec{r}). \tag{3}$$

By substituting (3) into the electric field volume integral equation, we can observe that the unknown currents $\vec{J}_S$ and $\vec{J}_V$ are what we will solve in the metal-dielectric composite problem.

The scattering field contributed from the surface current and volume current can be determined by (4) and (5), respectively [34],

$$\begin{aligned}\vec{E}^{sca}\left(\vec{r};\vec{J}_S\right) &= ik_0\eta\int_S \bar{G}\left(\vec{r},\vec{r}'\right)\vec{J}_S\left(\vec{r}'\right)dS' \\ &= ik_0\eta\int_S\left(g\left(\vec{r},\vec{r}'\right)\vec{J}_S\left(\vec{r}'\right)+\frac{1}{k_0^2}\nabla g\left(\vec{r},\vec{r}'\right)\nabla'\cdot\vec{J}_S\left(\vec{r}'\right)\right)dS' \end{aligned} \tag{4}$$

$$\begin{aligned}\vec{E}^{sca}\left(\vec{r};\vec{J}_V\right) &= ik_0\eta\int_V \bar{G}\left(\vec{r},\vec{r}'\right)\vec{J}_V\left(\vec{r}'\right)dV' \\ &= ik_0\eta\int_V\left(g\left(\vec{r},\vec{r}'\right)\vec{J}_V\left(\vec{r}'\right)+\frac{1}{k_0^2}\nabla g\left(\vec{r},\vec{r}'\right)\nabla'\cdot\vec{J}_V\left(\vec{r}'\right)\right)dV'. \end{aligned} \tag{5}$$

To solve the integral Equations (1) and (2) by the MoM, the entire structure should be meshed into small cells. In our simulation, the PEC surface is meshed into curvilinear triangle patches, and the same order curvilinear-faced tetrahedron cell is used to mesh the dielectric volume [6, 35]. The combination of triangle-tetrahedron mesh has great flexibility in the approximation of arbitrary shaped surface and volume. Next, the curvilinear Rao-Wilton-Glisson (CRWG) basis function is used to expand the surface current [36]. The 3D CRWG basis function defined over adjacent tetrahedrons is applied to expand the volume unknown $i\omega\vec{D}(\vec{r})$ [6]. The volume unknown selected here is

to ensure the continuity of the normal electric flux density $\vec{D}(\vec{r})$ across a dielectric interface. Therefore, the surface and volume currents can be expressed as the superposition of the basis functions, respectively

$$\vec{J}_S(\vec{r}) = \sum_{n=1}^{N_s} \alpha_n^s \vec{f}_n^S(\vec{r}) \tag{6}$$

$$\vec{J}_V(\vec{r}) = \chi(\vec{r}) i\omega \vec{D}(\vec{r}) = \chi(\vec{r}) \sum_{n=1}^{N_v} \alpha_n^v \vec{f}_n^V(\vec{r}) \tag{7}$$

where α_n^s and α_n^v stand for the expansion coefficients for the surface and volume current, respectively; N_s and N_v are the number of surface and volume basis functions, respectively. By substituting (6) and (7) into the two integral Equations (1) and (2), and applying the resultant equations by Galerkin's method, a set of linear equations can be obtained

$$\begin{bmatrix} Z^{SS} & Z^{SV} \\ Z^{VS} & Z^{VV} \end{bmatrix} \cdot \begin{bmatrix} \alpha^S \\ \alpha^V \end{bmatrix} = \begin{bmatrix} V^S \\ V^V \end{bmatrix} \tag{8}$$

where the block matrix $Z^{\Omega\Theta}$, Ω, $\Theta \in \{S, V\}$ contains the elements resulted from the testing of basis function $\vec{f}^{\Theta}(\vec{r})$ with $\vec{f}^{\Omega}(\vec{r})$; V^S and V^V are the excitation vectors corresponding to the surface and volume basis functions, respectively. By applying the vector identity, the divergence theory and the properties of the basis functions, formulations of the elements in the block matrices can be reduced to more compact forms. Formulations for the elements in the block matrices are presented in the Appendix A. Elements in the right hand side of (8) are also provided in the Appendix A.

2.2. The Modified Impedance Matrix

The matrix elements described in (A1)–(A4) represent the self-coupling and mutual coupling between the PEC surface and dielectric material, and they can be evaluated by numerical integration scheme directly. However, significant computational effort is required to fill the impedance matrix, especially in those highly frequency dependent problems, where frequency sweeps with fine increments are necessary to get accurate frequency responses.

On the other hand, the element formulations in (A1)–(A4) reveal that the frequency variations of all the impedance matrix elements are dominated by the phase term e^{ik_0R}, where $R = \left|\vec{r} - \vec{r}'\right|$. When the observation $\vec{r}$ and source $\vec{r}'$ are close to each other, R is small and

e^{ik_0R} varies slowly with frequency. When they are far from each other, the corresponding element fluctuates more rapidly as a function of the frequency. It can also be noted from (A1)–(A4) that if the phase term is factored out according to the distance R, each type of matrix element contains two frequency dependent terms: one is the linear term with k_0, and the other is the inverse term with coefficient $1/k_0$. For this reason, the following modified matrix elements are developed for the VSIE approach

$$\tilde{Z}_{mn}^{\Omega\Theta} = \begin{cases} Z_{mn}^{\Omega\Theta} f_r e^{-i2\pi f_r R_{mn}/\lambda_h}, & \Omega_m \cap \Theta_n = 0 \\ Z_{mn}^{\Omega\Theta} f_r, & \Omega_m \cap \Theta_n \neq 0 \end{cases}, \ \Omega, \ \Theta \in \{S, V\} \quad (9)$$

where $f_r = f_0/f_h$ is the normalized frequency, and it varies in the range $[f_l/f_h,1]$, λ_h is the free space wavelength at f_h; $[f_l, f_h]$ defines the frequency band of interest, and f_0 is the frequency sample in this range. The term $e^{-i2\pi f_r R_{mn}/\lambda_h}$ is multiplied to extract the domain phase term in the Green's function, where R_{mn} is the distance between centers of the meshed elements Ω_m and Θ_n. Therefore, only the remaining phase term $e^{i2\pi f_r/\lambda_h(R-R_{mn})}$ exists in the matrix elements, and it fluctuates slowly with the frequency. The matrix elements in (9) are multiplied with f_r, therefore, the linear term in $Z_{mn}^{\Omega\Theta}$ is converted to a quadratic term in $\tilde{Z}_{mn}^{\Omega\Theta}$, and the inverse term in $Z_{mn}^{\Omega\Theta}$ is converted to a frequency independent term.

As can be seen from (9), the domain phase term is extracted according to the physical layouts of the basis functions. Therefore, the criterion designed to determine whether one basis functions is the neighbor of another will dominate the accuracy, and it is essential to design a reasonable criterion. For the elements in block matrices Z^{SS} and Z^{VV}, the definition of the "neighboring elements" is the same as that in [32]. If the elements supporting the test function m and basis function n have at least one common element, we define $\Omega_m \cap \Theta_n \neq 0$; otherwise $\Omega_m \cap \Theta_n = 0$. However, the "neighboring elements" definition will be quite different for the elements in Z^{SV} and Z^{VS}, since the CRWG and 3D CRWG basis functions are defined over different types of cells. Supposing that the surface elements $S_m^{\pm}$ and volume elements $V_n^{\pm}$ are the elements corresponding to the test and basis functions in Z_{mn}^{SV}, respectively, if there is at least one common triangle elements between the curvilinear triangles $S_m^{\pm}$ and the faces of the tetrahedrons $V_n^{\pm}$, we define $\Omega_m \cap \Theta_n \neq 0$; otherwise $\Omega_m \cap \Theta_n = 0$. The definition of the "neighboring elements" for Z^{VS} is similar to that for Z^{SV}. The only difference is that the test and basis functions in Z^{VS} are defined over volume and surface elements, respectively. Based on these definitions, the domain phase terms in the four block matrices can be effectively extracted.

2.3. The Interpolation Scheme

Besides the remaining phase term, all the modified matrix elements in (A1)–(A4) only contain the quadratic terms, thus quadratic polynomial based interpolation methods may be suitable for the interpolating of the modified matrices at any frequency samples. However, the remaining phase term $e^{i2\pi f_r/\lambda_h(R-R_{mn})}$ retained in the modified matrix elements still varies with frequency, and it will weaken any quadratic polynomial based interpolation methods to some extent. Therefore, cubic polynomial based interpolation methods would produce more accurate results. For the integrity of this paper, the new interpolation method based on cubic polynomial employed in [32], which was proved to be more accurate than the Hermite interpolation scheme and Lagrange scheme, is introduced briefly in the following.

It is convenient to introduce the following variations: let x_0, x_1, x_2, and x represent the normalized frequencies f_l/f_h, f_{in}/f_h, f_h/f_h, and f_r, respectively, where f_{in} is the internal frequency in $[f_l,\ f_h]$; g(x_i) denotes the modified matrix elements at x_i, $i = 1,\ 2,\ 3$; $g'(x_1)$ is the first order derivative of $g(x_1)$, with respect to the normalized frequency.

The novel interpolation method in [32] begins by evaluating the modified matrices at three frequency samples f_l, f_{in}, and f_h directly as in the MoM. Moreover, the first order derivative of the modified matrix at f_{in} should also be computed before interpolation. The first order derivative of the modified matrix in VSIE is presented in the Appendix A. The modified matrix for any normalized intermediate frequencies f_r is then approximated by a cubic polynomial

$$g(x) = g(x_0)\phi_0(x) + g(x_1)\phi_1(x) + g(x_2)\phi_2(x) + g'(x_1)\xi_1(x) \tag{10}$$

where the polynomials associated with coefficients $g(x_i)$, $i = 1, 2, 3$ and $g'(x_1)$ can be easily obtained by matching the boundary conditions at x_0, x_1, and x_2

$$\phi_0(x) = \frac{x - x_2}{x_0 - x_2}\left(\frac{x - x_1}{x_0 - x_1}\right)^2 \tag{11}$$

$$\phi_1(x) = \frac{x - x_0}{x_1 - x_0}\cdot\frac{x - x_2}{x_1 - x_2}\left(1 - \frac{x - x_1}{x_1 - x_0} - \frac{x - x_1}{x_1 - x_2}\right) \tag{12}$$

$$\phi_2(x) = \frac{x - x_0}{x_2 - x_0}\left(\frac{x - x_1}{x_2 - x_1}\right)^2 \tag{13}$$

$$\xi_1(x) = (x - x_1)\frac{x - x_0}{x_1 - x_0}\cdot\frac{x - x_2}{x_1 - x_2}. \tag{14}$$

Once the modified matrix at any normalized intermediate frequency f_r is evaluated efficiently using the approximate formulation

in (10), the impedance matrix at the corresponding frequency $f_0 = f_r \times f_h$ can be easily calculated according to the inverse process of (9)

$$Z_{mn}^{\Omega\Theta} = \begin{cases} \tilde{Z}_{mn}^{\Omega\Theta} e^{i2\pi f_r R_{mn}/\lambda_h} \Big/ f_r, & \Omega_m \cap \Theta_n = 0 \\ \tilde{Z}_{mn}^{\Omega\Theta} \Big/ f_r, & \Omega_m \cap \Theta_n \neq 0 \end{cases}. \tag{15}$$

Since all the computational intensive integrations in (A1)–(A4) are replaced by a simple algebraic operation in (10), the filling time for the impedance matrix at any frequency sample of interest is significantly reduced. However, it is necessary to point out that the reduction in CPU time is at the cost of increased storage memory, since all the modified impedance matrices at f_l, f_{in}, f_h and the first order derivative of the modified impedance matrix at f_{in} need to be stored. For electrical large problems, special storage techniques introduced in [37] can be employed to alleviate the large memory requirement.

3. NUMERICAL RESULTS

In this section, numerical examples will be presented to show the capability of the proposed method. Specifically, the method is applied to a broadband U-slot patch antenna and two rectangular patch antennas in the first subsection. These antennas were chosen since they possess different substrate thickness and different resonant characters. In the second subsection, numerical results will be presented to illustrate the efficiency and interpolation bandwidth. Accuracy of the present method will be further validated from different aspects. In the numerical examples presented below, the internal frequency is always chosen to be the center frequency of the band, since the VSIEs in (1) and (2) are typical electric field integral equations (EFIE). The generalized minimal residual method (GMRES) is taken as the matrix solver throughout this paper, and a block diagonal preconditioning is involved to accelerate the convergence rate.

3.1. Applications in Microstrip Antenna Analysis

In the first example, a rectangular patch antenna printed on a finite size dielectric substrate is considered. Fig. 1 shows the configuration of the patch antenna (referred as Antenna #1), which is composed of a probe fed rectangular patch fabricated on a grounded substrate ($\varepsilon_r = 2.33$, $h = 1.57\,\text{mm}$, and $\tan\delta = 0.01$). An extended voltage gap feed with four feeding edges around the probe is employed to represent the excitation [38, 39]. In this feed model, two CRWG basis functions that share the same 'minus' curvilinear triangle element (on

the feed column) are defined across each of the feeding edges for the introduction of infinitesimally thin voltage gaps. The 'plus' curvilinear triangle elements of the two special CRWG basis functions are the one meshed from the ground plane and bottom of the feed column, respectively. This kind of special CRWG basis functions are also defined at the junction of the feed column and radiating patch. As compared to the simple voltage gap feed model, the extended one has the advantage that the feed structure in real-world is well described in the MoM meshes, and the electrical current at the feed point is supported by totally eight basis functions, thus the resultant input impedance would be more accurate than that from the simple voltage gap feed model [39]. In this paper, the extended voltage gap feed model is employed throughout all the probe fed microstrip antennas.

In Fig. 2, frequency response of the input impedance calculated using the present method is compared with the HFSS FEM simulation results and those calculated using traditional MoM. The HFSS FEM and traditional MoM simulation results are referred to as "FEM" and "Exact MoM", respectively. Since the efficiency of the impedance matrix filling is significantly improved in the interpolation method, a fine frequency increment of 5 MHz is considered for the interpolation method, while a large frequency step of 25 MHz is considered in the FEM and exact MoM results. Although the number of frequency samples is different among the three methods, one can still see the reasonable agreement in Fig. 2, in terms of both the real and imaginary parts of the input impedance. Fig. 3 presents the co-polar and cross-polar directivity patterns in the E-plane and H-plane at 2.35 GHz, good agreement is observed between the co-polar patterns calculated

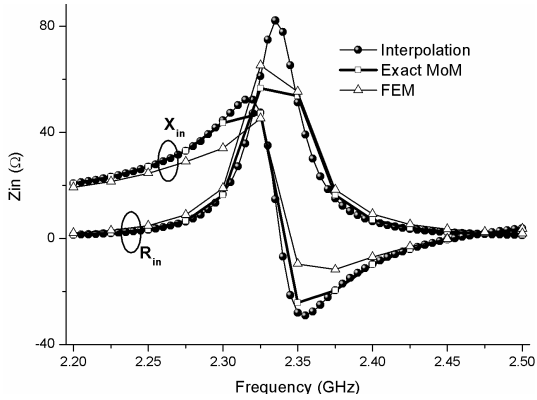

Figure 2. Simulated input impedances of Antenna #1 using the interpolation method, exact MoM and HFSS FEM.

by the interpolation method and HFSS. However, the discrepancy in the cross-polar patterns is relatively high, although the cross-polar level has been well predicted by the interpolation method. This is mainly due to the fact that both of the cross-polar levels in the E-plane and H-plane are below -30 dB, which are so low that they are more sensitive to various numerical errors.

In the second example, a rectangular patch antenna with thicker substrate is considered. Fig. 4 shows the configuration of this antenna (referred as Antenna #2). Again, the input impedances over a frequency band are compared. It can be seen from Fig. 5 that the results are also close to each other, although the internal frequency of 300 MHz is far away from the highly frequency dependent range 200–240 MHz. Fig. 6 compares the directivity patterns obtained from the interpolation method and HFSS FEM at 260 MHz. Unlike the case in Antenna #1, good agreement is observed, both in the co-polar and

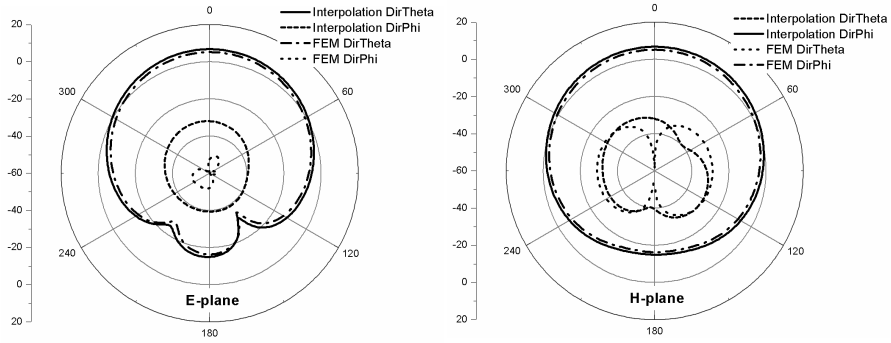

Figure 3. Comparison of the directivity patterns of the co-polar and cross-polar fields for Antenna #1. (a) E-plane; (b) H-plane.

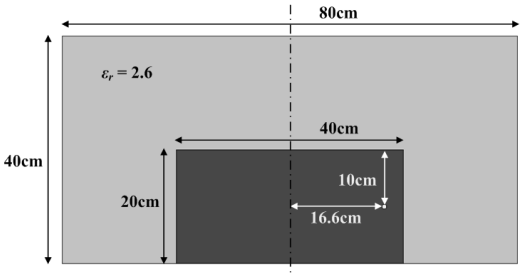

Figure 4. Configuration of a rectangular patch antenna with thicker substrate (Antenna #2).

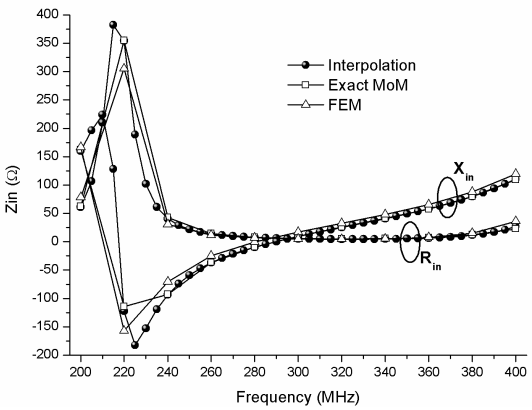

Figure 5. Simulated input impedance of Antenna #2 using the interpolation method, exact MoM and HFSS FEM.

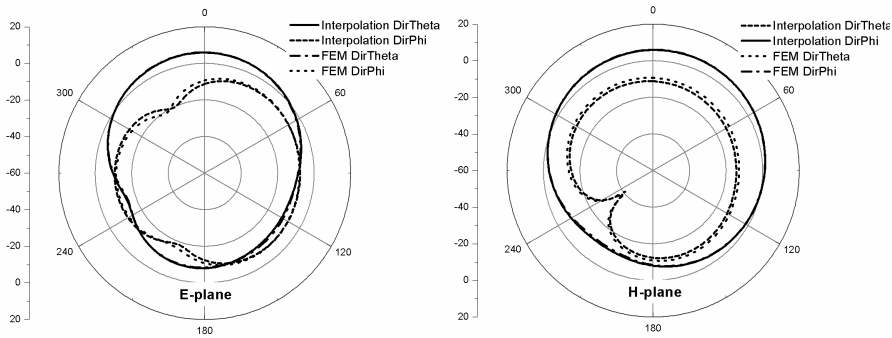

Figure 6. Comparison of the directivity patterns of the co-polar and cross-polar fields for Antenna #2. (a) E-plane; (b) H-plane.

cross-polar patterns. The good agreement in the cross-polar patterns is mainly due to the fact that the cross-polarization is relatively high.

Finally, we consider the application of the interpolation method in the analysis of a broadband U-slot rectangular patch antenna as shown in Fig. 7 (referred as Antenna #3), where there are totally 65 frequency samples considered. Both the measured and calculated input impedance and radiation patterns are available in published papers [40, 41]. It is interesting to note that the ground plane is larger than the substrate, which will improve the front-to-back ratio. Figs. 8(a) and (b) plot the input impedances in the Smith Chart and the reflection coefficient over the frequency band of 2.4–4.0 GHz, respectively. The input impedance agrees well with those calculated

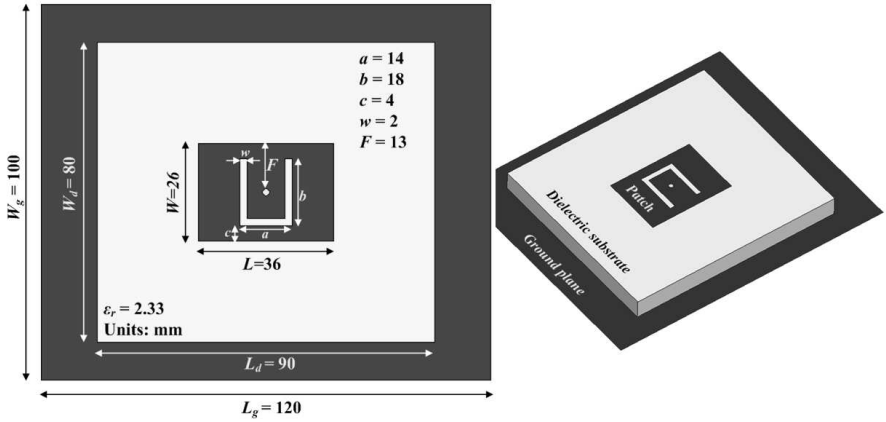

Figure 7. Configuration of the broadband U-slot rectangular patch antenna (Antenna #3).

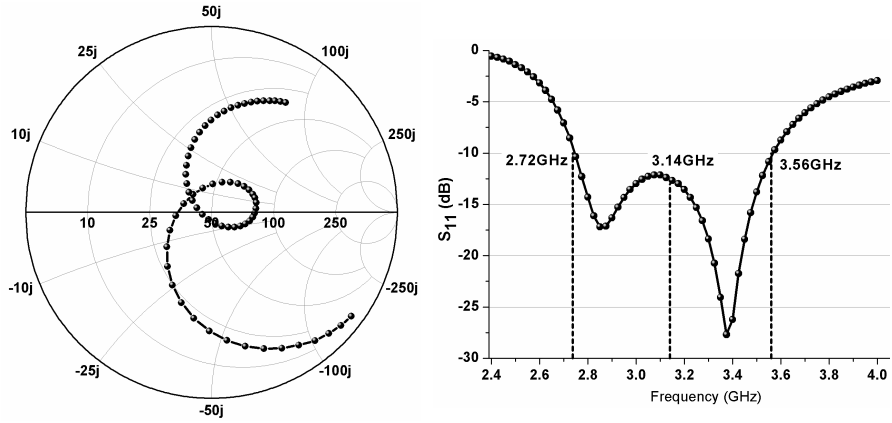

(a) (b)

Figure 8. Input impedance and reflection coefficient of Antenna #3. (a) Input impedance in the Smith Chart; (b) reflection coefficient.

and measured in [40, 41], especially within the operating frequency band ($S_{11} < -10$ dB). The reflection coefficient illustrates that the lower cutoff frequency, center frequency, and upper cutoff frequency of Antenna #3 locate at 2.72 GHz, 3.14 GHz, and 3.56 GHz, respectively, which are the same as those obtained from the finite-difference time-domain (FDTD) simulations [40]. Therefore, both the accuracy and effectiveness of the interpolation method and the extended feed model are further validated.

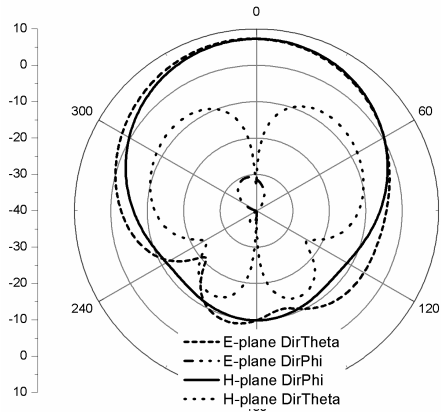

Figure 9. Directivity patterns of the co-polar and cross-polar fields for Antenna #3.

Figure 9 shows the co-polar and cross-polar directivity patterns at 2.68 GHz, where the cross-polar patterns have not been given in [40] and [41]. It can be clearly observed that the co-polar pattern in E-plane agrees very well with the measured data in [40] and calculated data in [41], which indicates that the pattern in the E-plane calculated by FDTD is inaccurate. For the co-polar pattern in H-plane, our results agree well with those calculated in [40, 41], which further demonstrate the claims in [41] that the measured data in the H-plane is not very accurate.

3.2. Performance of the Interpolation Method in VSIE

Firstly, efficiency of the interpolation method is verified by comparing the impedance matrix filling time with that using the conventional numerical integration method. Table 1 lists the unknowns, impedance matrix filling time of the numerical integration method and interpolation method in the examples presented in Section 3.1. The time denoted as "Computed Directly" is the impedance matrix filling time for a single frequency point when using the conventional numerical integration method, according to the formulations presented in (A1)–(A4). The time denoted as "interpolation" is the impedance matrix filling time for a single frequency point when using the interpolation method, according to the formulations presented in (10) and (15). As can be seen, the impedance matrix filling time of the interpolation method is at least 21 times less than that in the conventional MoM. The only cost in the interpolation method is the time consumed in

Table 1. Impedance matrix filling time in the interpolation method and direct MoM.

	Antenna #1	Antenna #2	Antenna #3
Number of Unknowns	5710	3114	4797
Computed Directly (Sec.)	1293	421	692
Interpolation (Sec.)	61	18	33

Table 2. Comparison of the impedance matrix elements with the modified impedance matrix elements in a 10 : 1 bandwidth.

	40 MHz	400 MHz
Z_{00}^{SS}	$-1167.05 + 6.5600e-06i$	$-116.643 + 0.0006655i$
$\tilde{Z}_{00}^{SS}$	$-93.3641 + 5.2480e-07i$	$-93.3145 + 0.0005324i$
$Z_{0,307}^{SV}$	$0.22767 + 4.47807e-6i$	$0.024321 + 0.000434i$
$\tilde{Z}_{0,307}^{SV}$	$0.0182001 - 0.000702i$	$0.0181596 - 0.006994i$

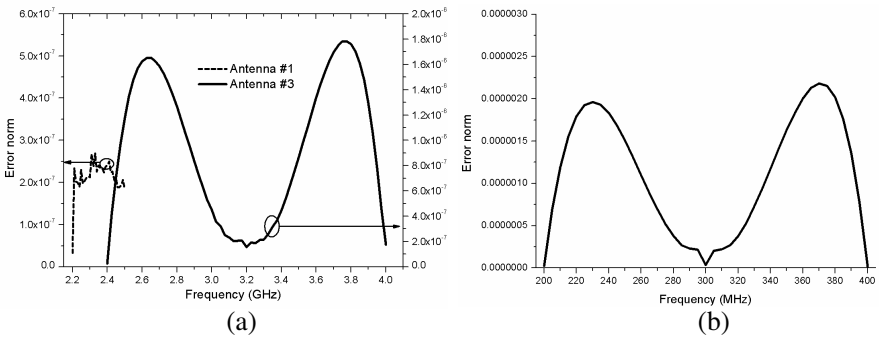

(a) (b)

Figure 10. Error norms of the interpolated impedance matrices for the antenna simulations. (a) Antenna #1 and #3; (b) Antenna #2.

the calculation of the derivative of the modified matrix elements at the internal frequency. However, when parameters at a large number of frequency points need to be calculated accurately, the time cost in the present method is negligible, thus the total time saved in the interpolation method is considerable.

Secondly, accuracy of the method is confirmed by examining the values of the impedance matrix elements and their modified correspondences. The investigation is carried out based on Antenna #2. Table 2 displays the values of two matrix elements at 40 MHz

and 400 MHz, one is the self-impedance element formed by testing a surface basis function with the same surface basis function, and the other is the interact-impedance element formed by testing the surface basis function with a volume basis function. It can be observed that by factoring out the domain phase term and multiplying the normalized frequency, the modified matrix elements are almost frequency independent in a 10 : 1 bandwidth, while the matrix elements fluctuate more rapidly as functions of the frequency. The good property of the modified matrix elements will guarantee the accuracy of the interpolation method. The accuracy can be revealed by investigating the error norms. As can be seen from Fig. 10, although the volume terms are considered in the integral equation, the error norms of the interpolated impedance matrices are comparable to the case in SIE [32]. Specifically, the error norm will be rather small when the interpolated frequency band is very narrow, such as the case in Antenna #1. The error norms in Fig. 10 also illustrate the rationality of the "neighboring elements" definitions in Section 2.2. Furthermore, the error norms in the VSIE formulations are as small as those in

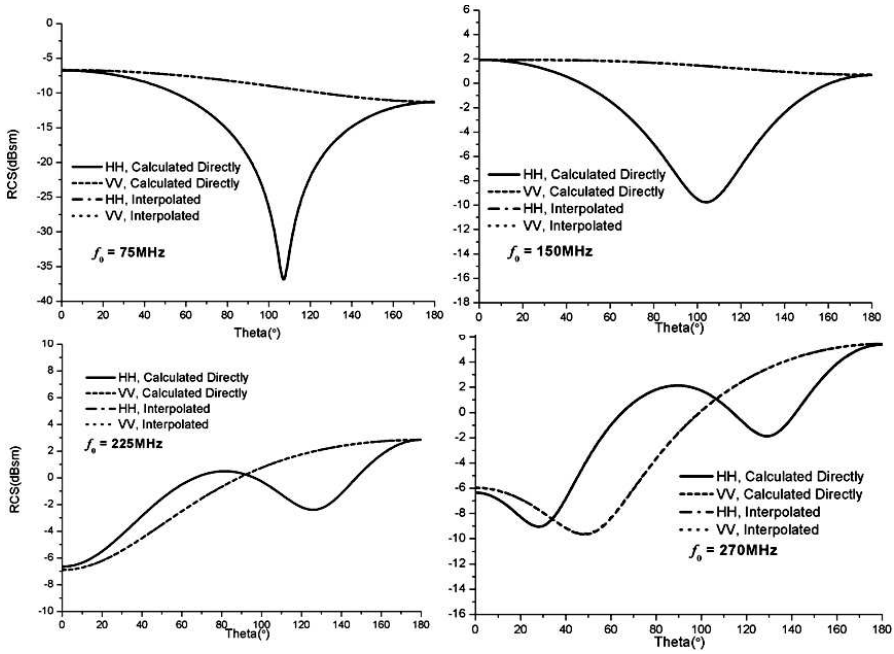

Figure 11. Bistatic RCS of a coated sphere at four interpolated frequency sample points.

the SIE, which demonstrates that if the domain phase term could be extracted effectively (or the definition of the neighboring elements is reasonable), the new interpolation scheme is independent of the basis functions.

Finally, to demonstrate the capability of the interpolation method in a wider frequency band, the bistatic radar cross section (RCS) of a coated sphere over a 10 : 1 bandwidth is considered. The conducting sphere has a radius of 0.3 m, and a homogeneous coating with a thickness of 0.05 m is around the core. The dielectric permittivity of the coating material is $\varepsilon_r = 4.0+0.01i$. In the interpolation method, f_l, f_{in}, and f_h are chose to be 30 MHz, 160 MHz, and 300 MHz, respectively. The bistatic RCS at four frequency samples, i.e., $f_0 = 75$ MHz, 150 MHz, 225 MHz, and 270 MHz, are compared with those calculated directly from MoM in Fig. 11. Excellent agreement between the results of the two methods is found, which demonstrates that the present method can be applied to a 10 : 1 bandwidth with high accuracy.

4. CONCLUSION

In this paper, an accurate analysis approach is developed to solve metal-dielectric composite radiation problems, using an extended impedance matrix interpolation technique. The contribution of this work is twofold. Firstly, the accurate impedance matrix interpolation technique proposed in [32] is extended to VSIE. Specifically, formulations of modified matrix and its first derivative in VSIE are derived, and an effective neighboring elements definition has been given. Secondly, the extended method is applied to the analysis of various microstrip antennas, in which fine frequency increment is generally necessary because they are highly frequency dependent. Great potential of the method would be found in the analysis of impulse antennas designed for the radiation of ultra-wideband (UWB) electromagnetic pulses, since responses over large number of frequency points are necessary for the getting of time domain responses. Besides, the accuracy, efficiency and the capability of the interpolation in wide bandwidth are also investigated by comparing the numerical results with measured data, exact MoM solutions, FEM solutions and FDTD solutions. Numerical results show that the proposed method is suitable for the analysis of wideband metal-dielectric composite problems with high accuracy.

ACKNOWLEDGMENT

This work was supported by the Natural Science Foundation of China under Grant (60971030), the New Century Excellent Talent Program in China under Grant (NCET-06-0809), and was also partially supported by the 111 Project of China under Grant (B07046).

APPENDIX A.

As stated in Section 2.1, by substituting Equations (4)–(7) into the coupled VSIEs (1) and (2), and applying the resultant equations by the Galerkin's method, a set of N_s+N_v linear equations are obtained in (8). By reorganizing the expressions of the impedance matrix elements using the vector identity, the divergence theory and properties of basis functions, the following elements in the block matrices can be obtained

$$\begin{aligned} Z_{mn}^{SS} &= k_0 \int\limits_{S_m^{\pm}} \int\limits_{S_n^{\pm}} \vec{\vec{f}}_m^{\,S}(\vec{r}) \cdot \vec{\vec{f}}_n^{\,S}\left(\vec{\vec{r}}'\right) g\left(\vec{r}, \vec{\vec{r}}'\right) dS' dS \\ &\quad - \int\limits_{S_m^{\pm}} \int\limits_{S_n^{\pm}} \nabla \cdot \vec{\vec{f}}_m^{\,S}(\vec{r}) \nabla' \cdot \vec{\vec{f}}_n^{\,S}\left(\vec{\vec{r}}'\right) g\left(\vec{r}, \vec{\vec{r}}'\right) \Big/ k_0 dS' dS \quad \text{(A1)} \end{aligned}$$

$$\begin{aligned} Z_{mn}^{SV} &= k_0 \int\limits_{S_m^{\pm}} \int\limits_{V_n^{\pm}} \vec{\vec{f}}_m^{\,S}(\vec{r}) \cdot \vec{\vec{f}}_n^{\,V}\left(\vec{\vec{r}}'\right) \chi\left(\vec{\vec{r}}'\right) g\left(\vec{r}, \vec{\vec{r}}'\right) dV' dS \\ &= - \int\limits_{S_m^{\pm}} \int\limits_{V_n^{\pm}} \nabla \cdot \vec{\vec{f}}_m^{\,S}(\vec{r}) \nabla' \cdot \vec{\vec{f}}_n^{\,V}\left(\vec{\vec{r}}'\right) \chi\left(\vec{\vec{r}}'\right) g\left(\vec{r}, \vec{\vec{r}}'\right) \Big/ k_0 dV' dS \\ &\quad + \int\limits_{S_m^{\pm} S_n} \int \nabla \cdot \vec{\vec{f}}_m^{\,S}(\vec{r}) \hat{n}' \cdot \vec{\vec{f}}_n^{\,V}\left(\vec{\vec{r}}'\right) \left(\chi_n^{+} - \chi_n^{-}\right) g\left(\vec{r}, \vec{\vec{r}}'\right) \Big/ k_0 dS' dS \quad \text{(A2)} \end{aligned}$$

$$\begin{aligned} Z_{mn}^{VS} &= k_0 \int\limits_{V_m^{\pm}} \int\limits_{S_n^{\pm}} \vec{\vec{f}}_m^{\,V}(\vec{r}) \cdot \vec{\vec{f}}_n^{\,S}\left(\vec{\vec{r}}'\right) g\left(\vec{r}, \vec{\vec{r}}'\right) dS' dV \\ &\quad - \int\limits_{V_m^{\pm}} \int\limits_{S_n^{\pm}} \nabla \cdot \vec{\vec{f}}_m^{\,V}(\vec{r}) \nabla' \cdot \vec{\vec{f}}_n^{\,S}\left(\vec{\vec{r}}'\right) g\left(\vec{r}, \vec{\vec{r}}'\right) \Big/ k_0 dS' dV \\ &\quad + \int\limits_{S_m} \int\limits_{S_n^{\pm}} \hat{n} \cdot \vec{\vec{f}}_m^{\,V}(\vec{r}) \nabla' \cdot \vec{\vec{f}}_n^{\,S}\left(\vec{\vec{r}}'\right) g\left(\vec{r}, \vec{\vec{r}}'\right) \Big/ k_0 dS' dS \quad \text{(A3)} \end{aligned}$$

$$
\begin{aligned}
Z_{mn}^{VV} &= 4\pi \int\limits_{V_m^{\pm}} \vec{f}_m^{V}(\vec{r}) \cdot \vec{f}_n^{V}(\vec{r}) \Big/ \varepsilon_r(\vec{r}) \Big/ k_0 dV \\
&+ k_0 \int\limits_{V_m^{\pm}} \int\limits_{V_n^{\pm}} \vec{f}_m^{V}(\vec{r}) \cdot \vec{f}_n^{V}\left(\vec{r}'\right) \chi\left(\vec{r}'\right) g\left(\vec{r}, \vec{r}'\right) dV' dV \\
&- \int\limits_{V_m^{\pm}} \int\limits_{V_n^{\pm}} \nabla \cdot \vec{f}_m^{V}(\vec{r}) \nabla' \cdot \vec{f}_n^{V}\left(\vec{r}'\right) \chi\left(\vec{r}'\right) g\left(\vec{r}, \vec{r}'\right) \Big/ k_0 dV' dV \\
&+ \int\limits_{V_m^{\pm}} \int\limits_{S_n} \nabla \cdot \vec{f}_m^{V}(\vec{r}) \hat{n}' \cdot \vec{f}_n^{V}\left(\vec{r}'\right) \left(\chi_n^{+} - \chi_n^{-}\right) g\left(\vec{r}, \vec{r}'\right) \Big/ k_0 dS' dV \\
&+ \int\limits_{S_m} \int\limits_{V_n^{\pm}} \hat{n} \cdot \vec{f}_m^{V}(\vec{r}) \nabla' \cdot \vec{f}_n^{V}\left(\vec{r}'\right) \chi\left(\vec{r}'\right) g\left(\vec{r}, \vec{r}'\right) \Big/ k_0 dV' dS \\
&- \int\limits_{S_m} \int\limits_{S_n} \hat{n} \cdot \vec{f}_m^{V}(\vec{r}) \hat{n}' \cdot \vec{f}_n^{V}\left(\vec{r}'\right) \left(\chi_n^{+} - \chi_n^{-}\right) g\left(\vec{r}, \vec{r}'\right) \Big/ k_0 dS' dS \quad \text{(A4)}
\end{aligned}
$$

where $g(\vec{r}, \vec{r}') = e^{ik_0\left|\vec{r}-\vec{r}'\right|} \Big/ \left|\vec{r} - \vec{r}'\right|$ is the scalar Green's function in free space, k_0 is the wave number at the frequency $f_0$in free space, $\chi^{\pm}$ is the contrast ratio at each side of the common surface, $\hat{n}$ and $\hat{n}'$ are the unit normal vector point from 'plus' elements to 'minus' elements; the integral domain with subscripts 'm' and 'n' are the supports of the testing and basis functions, respectively; the integral domain S_m and S_n stand for the closed surfaces on which 'half' volume basis functions are defined.

The corresponding elements in the excitation vectors are given by

$$V_m^S = \frac{4\pi i}{\eta} \int\limits_{S_m^{\pm}} \vec{f}_m^{S}(\vec{r}) \vec{E}^{i}(\vec{r}) dS \quad \text{(A5)}$$

$$V_m^V = \frac{4\pi i}{\eta} \int\limits_{V_m^{\pm}} \vec{f}_m^{V}(\vec{r}) \vec{E}^{i}(\vec{r}) dV. \quad \text{(A6)}$$

The cubic polynomial based interpolation method introduced in Section 2.3 requires the first order derivative of the modified matrix elements. It is easy to get the general form of the first order derivative with respect to f_r in the following two cases

a). $\Omega_m \cap \Theta_n = 0$:

$$\left(\tilde{Z}_{mn}^{\Omega\Theta}\right)' = \left[\left(Z_{mn}^{\Omega\Theta} f_r\right)' - \frac{i2\pi R_{mn}}{\lambda_h} Z_{mn}^{\Omega\Theta} f_r\right] e^{-i2\pi f_r R_{mn}/\lambda_h} \tag{A7}$$

b). $\Omega_m \cap \Theta_n \neq 0$:

$$\left(\tilde{Z}_{mn}^{\Omega\Theta}\right)' = \left(Z_{mn}^{\Omega\Theta} f_r\right)'. \tag{A8}$$

It is observed that once the first order derivative of $Z_{mn}^{\Omega\Theta} f_r$ is obtainable, derivatives of the modified matrix elements in the two cases can be easily evaluated. Since $Z_{mn}^{\Omega\Theta} f_r$ is continuously differentiable with respect to f_r, its first order derivative can be written as an explicit expression. Formulations of the first order derivative of $Z_{mn}^{SS} f_r$, $Z_{mn}^{SV} f_r$, $Z_{mn}^{VS} f_r$, and $Z_{mn}^{VV} f_r$ are presented in (A9)–(A12), respectively

$$\begin{aligned}\left(Z_{mn}^{ss} f_r\right)' = &-i \int\limits_{S_m^{\pm}} \int\limits_{S_n^{\pm}} \nabla \cdot \vec{f}_m^{\,S}(\vec{r}) \nabla' \cdot \vec{f}_n^{\,S}\left(\vec{r}'\right) e^{i2\pi f_r R/\lambda_h} dS' dS \\ &+ \frac{2\pi f_r}{\lambda_h} \int\limits_{S_m^{\pm}} \int\limits_{S_n^{\pm}} \vec{f}_m^{\,S}(\vec{r}) \cdot \vec{f}_n^{\,S}\left(\vec{r}'\right) e^{i2\pi f_r R/\lambda_h} \left(\frac{2}{R} + \frac{i2\pi f_r}{\lambda_h}\right) dS' dS \end{aligned} \tag{A9}$$

$$\begin{aligned}\left(Z_{mn}^{SV} f_r\right)' = &-i \int\limits_{S_m^{\pm}} \int\limits_{V_n^{\pm}} \nabla \cdot \vec{f}_m^{\,S}(\vec{r}) \nabla' \cdot \vec{f}_n^{\,V}\left(\vec{r}'\right) \chi\left(\vec{r}'\right) e^{i2\pi f_r R/\lambda_h} dV' dS \\ &+ i \int\limits_{S_m^{\pm}} \int\limits_{S_n} \nabla \cdot \vec{f}_m^{\,S}(\vec{r}) \hat{n}' \cdot \vec{f}_n^{\,V}\left(\vec{r}'\right) \left(\chi_n^{+} - \chi_n^{-}\right) e^{i2\pi f_r R/\lambda_h} dS' dS \\ &+ \frac{2\pi f_r}{\lambda_h} \int\limits_{S_m^{\pm}} \int\limits_{V_n^{\pm}} \vec{f}_m^{\,S}(\vec{r}) \cdot \vec{f}_n^{\,V}\left(\vec{r}'\right) \chi\left(\vec{r}'\right) e^{i2\pi f_r R/\lambda_h} \left(\frac{2}{R} + \frac{i2\pi f_r}{\lambda_h}\right) dV' dS \end{aligned} \tag{A10}$$

$$\begin{aligned}\left(Z_{mn}^{VS} f_r\right)' = &-i \int\limits_{V_m^{\pm}} \int\limits_{S_n^{\pm}} \nabla \cdot \vec{f}_m^{\,V}(\vec{r}) \nabla' \cdot \vec{f}_n^{\,S}\left(\vec{r}'\right) e^{i2\pi f_r R/\lambda_h} dS' dV \\ &+ i \int\limits_{S_m} \int\limits_{S_n^{\pm}} \hat{n} \cdot \vec{f}_m^{\,V}(\vec{r}) \nabla' \cdot \vec{f}_n^{\,S}\left(\vec{r}'\right) e^{i2\pi f_r R/\lambda_h} dS' dS \\ &+ \frac{2\pi f_r}{\lambda_h} \int\limits_{V_m^{\pm}} \int\limits_{S_n^{\pm}} \vec{f}_m^{\,V}(\vec{r}) \cdot \vec{f}_n^{\,S}\left(\vec{r}'\right) e^{i2\pi f_r R/\lambda_h} \left(\frac{2}{R} + \frac{i2\pi f_r}{\lambda_h}\right) dS' dV \end{aligned} \tag{A11}$$

$$\left(Z_{mn}^{VV}\cdot f_r\right)' = -i\int\limits_{V_m^{\pm}}\int\limits_{V_n^{\pm}} \nabla\cdot\vec{f}_m^{\,V}(\vec{r})\nabla'\cdot\vec{f}_n^{\,V}\left(\vec{r}'\right)\chi\left(\vec{r}'\right)e^{i2\pi f_r R/\lambda_h}dV'dV$$

$$+i\int\limits_{V_m^{\pm}}\int\limits_{S_n} \nabla\cdot\vec{f}_m^{\,V}(\vec{r})\hat{n}'\cdot\vec{f}_n^{\,V}\left(\vec{r}'\right)\left(\chi_n^{+}-\chi_n^{-}\right)e^{i2\pi f_r R/\lambda_h}dS'dV$$

$$+i\int\limits_{S_m}\int\limits_{V_n^{\pm}} \hat{n}\cdot\vec{f}_m^{\,V}(\vec{r})\nabla'\cdot\vec{f}_n^{\,V}\left(\vec{r}'\right)\chi\left(\vec{r}'\right)e^{i2\pi f_r R/\lambda_h}dV'dS$$

$$-i\int\limits_{S_m}\int\limits_{S_n} \hat{n}\cdot\vec{f}_m^{\,V}(\vec{r})\hat{n}'\cdot\vec{f}_n^{\,V}\left(\vec{r}'\right)\left(\chi_n^{+}-\chi_n^{-}\right)e^{i2\pi f_r R/\lambda_h}dS'dS$$

$$+\frac{2\pi f_r}{\lambda_h}\int\limits_{V_m^{\pm}}\int\limits_{V_n^{\pm}} \vec{f}_m^{\,V}(\vec{r})\cdot\vec{f}_n^{\,V}\left(\vec{r}'\right)\chi\left(\vec{r}'\right)\left(\frac{2}{R}+\frac{i2\pi f_r}{\lambda_h}\right)e^{i2\pi f_r R/\lambda_h}dV'dV \quad \text{(A12)}$$

REFERENCES

1. Harrington, R. F., *Field Computation by Moment Methods*, IEEE Press, New York, 1993.
2. Chew, W. C., J. Jin, C. Lu, E. Michielssen, and J. M. Song, "Fast solution methods in electromagnetics," *IEEE Trans. Antennas Propagat.*, Vol. 45, No. 3, 533–543, Mar. 1997.
3. Chew, W. C. and Q. H. Liu, "Resonance frequency of a rectangular microstrip patch," *IEEE Trans. Antennas Propagat.*, Vol. 36, No. 8, 1045–1056, Aug. 1988.
4. Wilton, D. R., "Review of current status and trends in the use of integral equations in computational electromagnetics," *Electromagn.*, Vol. 12, 287–341, 1992.
5. Chen, C. and N. G. Alexopoulos, "Modeling microstrip line fed slot antennas with arbitrary shape," *Electromagn.*, Vol. 15, No. 5, 567–586, Sept./Oct. 1995.
6. Lu, C. C., "Volume-surface integral equation," *Fast and Efficient Algorithms in Computational Electromagnetics*, W. C. Chew, J. M. Jin, E. Michielssen, and J. M. Ming (eds.), 487–540, Artech House, Norwood, MA, 2001.
7. Ebadi, S. and K. Forooraghi, "Green's function derivation of an annular waveguide for application in method of moment analysis of annular waveguide slot antennas," *Progress In Electromagnetics Research*, Vol. 89, 101–119, 2009.
8. Papakanellos, P. J., "Accuracy and complexity assessment of sub-

domain moment methods for arrays of thin-wire loops," *Progress In Electromagnetics Research*, Vol. 78, 1–15, 2008.

9. Lashab, M., F. Benabdelaziz, and C.-E. Zebiri, "Analysis of electromagnetics scattering from reflector and cylindrical antennas using wavelet-based moment method," *Progress In Electromagnetics Research*, Vol. 76, 357–368, 2007.
10. Zhao, J., W. C. Chew, C. Lu, E. Michielssen, and J. Song, "Thin-stratified medium fast-multipole algorithm for solving microstrip structures," *IEEE Trans. Microwave Theory Tech.*, Vol. 46, No. 4,395–403, Apr. 1998.
11. Millard, X. and Q. H. Liu, "A fast volume integral equation solver for electromagnetic scattering from large inhomogeneous objects in planarly layered media," *IEEE Trans. Antennas Propagat.*, Vol. 51, No. 9, 2393–2401, Sep. 2003.
12. Yeo, J. and R. Mittra, "An algorithm for interpolating the frequency variations of method-of-moments matrices arising in the analysis of planar microstrip structures," *IEEE Trans. Microwave Theory Tech.*, Vol. 51, No. 3, 1018–1025, Mar. 2003.
13. Liu, Z.-F., P.-S. Kooi, L.-W. Li, M.-S. Leong, and T.-S. Yeo, "A method of moments analysis of a microstrip phased array in three-layered structures," *Progress In Electromagnetics Research*, Vol. 31, 155–179, 2001.
14. Li, L.-W., Y. Dan, M.-S. Leong, T.-S. Yeo, and J. A. Kong, "Plane wave scattering by an achiral multilayered sphere in an infinitely extended chiral host medium," *Progress In Electromagnetics Research*, Vol. 33, 261–298, 2001.
15. Poggio, A. J. and E. K. Miller, *Integral Equation Solution of Three Dimensional Scattering Problems*, Permagon, Elmsford, NY, 1973.
16. Chang, Y. and R. F. Harrington, "A surface formulation for characteristic modes of material bodies," *IEEE Trans. Antennas Propagat.*, Vol. 25, 789–795, 1977.
17. Wu, T. K. and L. L. Tsai, "Scattering from arbitrarily-shaped lossy dielectric bodies of revolution," *Radio Science*, Vol. 12, 709–718, 1977.
18. Ylä-Oijala, P., M. Taskinen, and J. Sarvas, "Surface integral equation method for general composite metallic and dielectric structures with junctions," *Progress In Electromagnetics Research*, Vol. 52, 81–108, 2005.
19. Mohsen, A. A. K. and A. K. Abdelmageed, "The uniqueness problem of the surface integral equations of a conducting body in a layered medium," *Progress In Electromagnetics Research*, Vol. 23,

277–300, 1999.

20. Usner, B. C., "Generalized hybrid methods for modeling complex electromagnetic structures," Ph.D. dissertation, The Ohio State University, 2006.
21. Sarkar, T. K., S. M. Rao, and A. R. Djordjević, "Electromagnetic scattering and radiation from finite microstrip structures," *IEEE Trans. Microwave Theory Tech.*, Vol. 38, No. 11, 1568–1575, Nov. 1990.
22. Rao, S. M., C. C. Cha, R. L. Cravey, and D. L. Wilkes, "Electromagnetic scattering from arbitrary shaped conducting bodies coated with lossy materials of arbitrary thickness," *IEEE Trans. Antennas Propagat.*, Vol. 39, No. 5, 627–631, May 1991.
23. Kishk, A. A., A. W. Glisson, and P. M. Goggans, "Scattering from conductors with materials of arbitrary thickness," *IEEE Trans. Antennas Propagat.*, Vol. 40, No. 1, 108–111, Jan. 1992.
24. Medgyesi-Mitschang, L. N., J. M. Putnam, and M. B. Gedera, "Generalized method of moments for three-dimensional penetrable scatterers," *J. Opt. Soc. of Amer. A*, Vol. 11, No. 4, 1383–1398, Apr. 1994.
25. Kolundžija, B. M., "Electromagnetic modeling of composite metallic and dielectric structures," *IEEE Trans. Microwave Theory Tech.*, Vol. 47, No. 7, 1021–1032, Jul. 1999.
26. He, S., Z. Nie, J. Wei, and J. Hu, "A highly efficient numerical solution for dielectric-coated PEC targets," *Waves in Random and Complex Media*, Vol. 19, No. 1, 65–79, Feb. 2009.
27. Virga, K. L. and Y. Rahmat-Samii, "Efficient wide-band evaluation of mobile communications antennas using $[Z]$ or $[Y]$ matrix interpolation with the method of moments," *IEEE Trans. Antennas Propagat.*, Vol. 47, No. 1, 65–76, Jan. 1999.
28. Newman, E. H. and D. Forrai, "Scattering from a microstrip patch," *IEEE Trans. Antennas Propagat.*, Vol. 35, No. 3, 245–251, Mar. 1987.
29. Karwowski, A. and A. Noga, "On the interpolation of the frequency variations of the MoM-PO impedance matrix over a wide bandwidth," *Microw. Opt. Technol. Lett.*, Vol. 50, No. 3, 738–741, Mar. 2008.
30. Zhou, H. X. and W. Hong, "Fast generation of $[Z]$ matrix in the method of moments over a wide frequency band by means of Hermite polynomial interpolation," *Proc. Asia-Pacific Microw. Conf. (APMC' 02)*, Vol. 2, 1196–1199, Kyoto, Japan, Nov. 19–22, 2002.

31. Newman, E. H., "Generation of wide-band data from the method of moments by interpolating the impedance matrix," *IEEE Trans. Antennas Propag.*, Vol. 36, No. 12, 1820–1824, Dec. 1988.
32. Li, W., H. Zhou, W. Hong, and T. Weiland, "An accurate interpolation scheme with derivative term for generating MoM matrices in frequency sweeps," *IEEE Trans. Antennas Propagat.*, Vol. 57, No. 8, 2376–2385, Aug. 2009.
33. Gennarelli, C., G. Riccio, C. Savarese, and V. Speranza, "Fast and accurate interpolation of radiated fields over a cylinder," *Progress In Electromagnetics Research*, Vol. 8, 349–375, 1994.
34. Zeng, Z. and C. C. Lu, "Discretization of hybrid VSIE using mixed mesh elements with zeroth-order galerkin basis functions," *IEEE Trans. Antennas Propagat.*, Vol. 54, No. 6, 1863–1870, Jun. 2006.
35. Wandzura, S., "Electric current basis functions for curved surfaces," *Electromagn.*, Vol. 12, No. 1, 77–91, Jan. 1992.
36. Rao, S. M., D. R. Wilton, and A. W. Glisson, "Electromagnetic scattering by surfaces of arbitrary shape," *IEEE Trans. Antennas Propagat.*, Vol. 30, No. 3, 409–418, May 1982.
37. Havé, P., "A parallel implementation of the fast multipole method for Maxwell's equations," *Int. J. Numer. Meth. Fluid*, Vol. 43, 839–864, 2003.
38. Makarov, S., S. Kulkarni, A. Marut, and L. Kempel, "Method of moments solution for a printed patch/slot antenna on a thin finite dielectric substrate using the volume integral equation," *IEEE Trans. Antennas Propagat.*, Vol. 54, No. 4, 1174–1184, Apr. 2006.
39. Makarov, S., S. Kulkarni, A. Marut, and L. Kempel, "Design and analysis of wideband planar monopole antennas using the multilevel fast multipole algorithm," *Progress In Electromagnetics Research B*, Vol. 15, 95–112, 2009.
40. Tong, K., K. Luk, K. Lee, and R. Lee, "A broad-band U-slot rectangular patch antenna on a microwave substrate," *IEEE Trans. Antennas Propagat.*, Vol. 48, No. 6, 954–960, Jun. 2000.
41. Yuan, N., T. Yeo, X. Nie, Y. Gan, and L. Li, "Analysis of probe-fed conformal microstrip antennas on finite grounded substrate," *IEEE Trans. Antennas Propagat.*, Vol. 54, No. 2, 554–563, Feb. 2006.